Anharmonic Phonon Lifetimes in Carbon Nanotubes: Evidence for a One-Dimensional Phonon Decay Bottleneck

Rahul Rao,[1] José Menendez,[2] Christian D. Poweleit,[2] and Apparao M. Rao[1]

[1]*Department of Physics and Astronomy, Clemson University, Clemson, South Carolina, 29634, USA*
[2] *Department of Physics and Astronomy, Arizona State University, Tempe, Arizona 85287, USA*

(Received 26 October 2006; published 26 July 2007)

High-resolution Raman spectroscopy is applied to suspended single-walled carbon nanotubes (SWNTs) to elucidate the puzzling differences in the lifetime of the radial breathing mode (RBM) obtained from different experimental techniques. Whereas recent tunneling experiments suggest a room temperature RBM lifetime as long as 10 ns , previous Raman experiments yield lifetimes shorter than 2 ps. The lifetimes obtained in this study are longer than 5 ps—a significant step in the direction of the tunneling results. We argue that the remaining discrepancy is due to the existence of phonon decay bottlenecks caused by the one-dimensional nature of nanotubes. Numerical simulations of the RBM decay show that it is possible to reconcile the short lifetimes measured spectroscopically with the long lifetimes obtained in tunneling experiments.

DOI: 10.1103/PhysRevLett.99.047403 PACS numbers: 78.67.Ch, 78.30.Na, 78.40.Ri

The study of elementary excitations in reduced-dimensionality systems has been one of the hallmarks of condensed matter physics for the past 30 years. Research on low-dimensional systems has also addressed the effect of dimensionality on the *interactions* between elementary excitations. Until now, these studies have focused on the electron-electron and electron-phonon interactions, but the anharmonic interaction between phonons has received much less attention. The relative lack of work on phonon-phonon interactions is understandable if one considers that the first accurate calculation of the Raman linewidth in simple bulk materials was published only a decade ago [1]. Moreover, anharmonic interactions often involve acoustic phonons, which are not as easy to confine as electrons and optical phonons. This state of affairs has changed dramatically with the development of spectroscopic techniques that probe individual semiconductor nanowires or carbon nanotubes. Intriguing results have begun to emerge [2–5]. Recent scanning tunneling microscopy (STM) experiments show that electrons tunneling into a metallic single-walled carbon nanotube (SWNT) induce the establishment of a nonequilibrium phonon population for the radial breathing mode (RBM) [2]. From these experiments, the anharmonic lifetime of the RBM was estimated to be $\tau \approx 10$ ns. This corresponds to a Raman full width at half maximum (FWHM) of 5×10^{-4} cm^{-1}, almost 4 orders of magnitude smaller than the observed FWHMs of 3 cm^{-1} ($\tau = 1.8$ ps) [3,5]. The instrumental line broadening in Raman instrumentation makes it impossible to measure intrinsic linewidths of 10^{-4} cm^{-1}, but the long lifetimes corresponding to narrow linewidths are easy to measure in the time domain. However, experiments detecting the coherent vibrations of RBM modes are consistent with a Raman FWHM of 3 cm^{-1} [6]. Therefore, the discrepancy of more than three-orders of magnitude between the tunneling and optical experiments is real, and suggests that the standard theoretical framework for analyzing anharmonic processes need revision in the case of one-dimensional (1D) carbon nanotubes.

In this Letter, we discuss room temperature, high-resolution micro-Raman measurements of suspended SWNTs which indicate that the FWHM for the RBM can be as small as 0.7 cm^{-1}, and it is in all cases substantially smaller than previously reported RBM linewidths. We also propose a model that explains the remaining large discrepancy with the tunneling results based on the unique properties of anharmonic systems in one dimension.

Suspended SWNTs were prepared via a chemical vapor deposition (CVD) method on etched silicon substrates. Trenches measuring 5 μm wide, 10 μm in length, and 3 μm in depth were etched in silicon substrates using focused ion beam microscopy. Individual suspended SWNTs were then grown across these trenches using the ''rapid-heating'' method [7]. The samples were characterized with scanning electron microscopy, which shows clear evidence of tubes extending across the trenches. Room temperature Raman spectra from suspended SWNTs were obtained in a backscattering geometry by focusing the 647.1 nm line from a Kr-ion laser using a 50× objective. The scattered light was dispersed using an ISA TRIAX 550 spectrometer. A spectral resolution better than 1 cm^{-1} was achieved with a slit size of 50 μm and a 2400 grooves/mm diffraction grating.

Figure 1 shows Raman spectra displaying a single RBM peak from metallic (panel a) and semiconducting (panel b) SWNTs. These spectra are assigned to single SWNTs. In a few cases, we also observe spectra with more than one RBM peak, which we assign to multiple or bundled tubes. The Raman line shapes were fit with a Voigt profile in which the Gaussian width component was determined from the laser line. From these fits we extract the

 © 2007 The American Physical Society

Lorentzian FWHM 2Γ, which turns out to be of the same order of magnitude as the spectral resolution. A similar analysis of the E_2 (low) Raman peak in ZnO shows that our deconvolution method can detect Lorentzian line widths that are 1/20th of the spectral resolution, so that the deconvolved nanotube linewidths are well above the technique's detection limit. The FWHM from several SWNTs is plotted against the corresponding RBM frequency in Fig. 2. Note that our linewidths are about 3 times smaller than any of the previously reported linewidths. To the best of our knowledge, a comparable linewidth was measured at a *low* temperature (20 K) for the RBM of the inner tube in a double-walled carbon nanotube [8]. However, the measured linewidths are still much larger than expected from the tunneling measurements.

Because of the remaining large discrepancy with the tunneling experiments, it is important to ascertain to what extent the Raman linewidths are intrinsic. The main contribution to the broadening of optical phonons is usually a down-conversion decay process of the form [9]

$$\Gamma(T) = \sum_{k\sigma\sigma'} \Gamma_{k\sigma\sigma'}[1 + n(\omega_{k\sigma}) + n(\omega_{-k\sigma'})] \times \delta(\omega_{\mathrm{RBM}} - \omega_{k\sigma} - \omega_{-k\sigma'}). \quad (1)$$

This involves the decay of the RBM into pairs of phonons $(\omega_{k\sigma}, \omega_{k'\sigma'})$ from branches σ and σ'. The functions $n(\omega)$ are the standard thermal occupation factors, and the coefficients $\Gamma_{k\sigma\sigma'}$ are proportional to the square of the anharmonic interaction matrix elements. The delta function in Eq. (1) implies that the linewidth is sensitive to the details of the phonon density of states whenever this density is highly structured, as in the case of SWNTs. Thus we do not expect a smooth dependence of the linewidths on diameter (or equivalently, on the RBM frequency), and Fig. 2 is consistent with this analysis.

A second implication from Eq. (1) is that the observed linewidth should depend on temperature. Conversely, if the true anharmonic linewidth was closer to 10^{-4} cm^{-1}, the temperature dependence would not be detectable. To decide this critical issue we measured Raman spectra for several SWNTs as a function of the laser power (Fig. 1). For typical values of ω_{RBM} Eq. (1) leads—at room and higher temperatures—to the approximate relationship $d\Gamma/dT = \Gamma/T$. We combine this result with the heat transport model of Ref. [10], adapted to the case of illumination with a laser beam of total power P. We assume that the maximum of the laser (TEM_{00}) power profile with FWHM $2r_0$ lies at the center of the suspended tube, and we set the nanotube thermal conductivity κ as 3600 W m^{-1} K^{-1} [11]. We find that the Raman linewidth as a function of laser power is approximately given by

$$\Gamma(P) = \Gamma(P_0)\frac{T_0 + kP}{T_0 + kP_0}. \quad (2)$$

Here T_0 is the boundary value temperature at the points $(-L/2, L/2)$, where the tube contacts the substrate, P_0 is a reference power, and k is given by

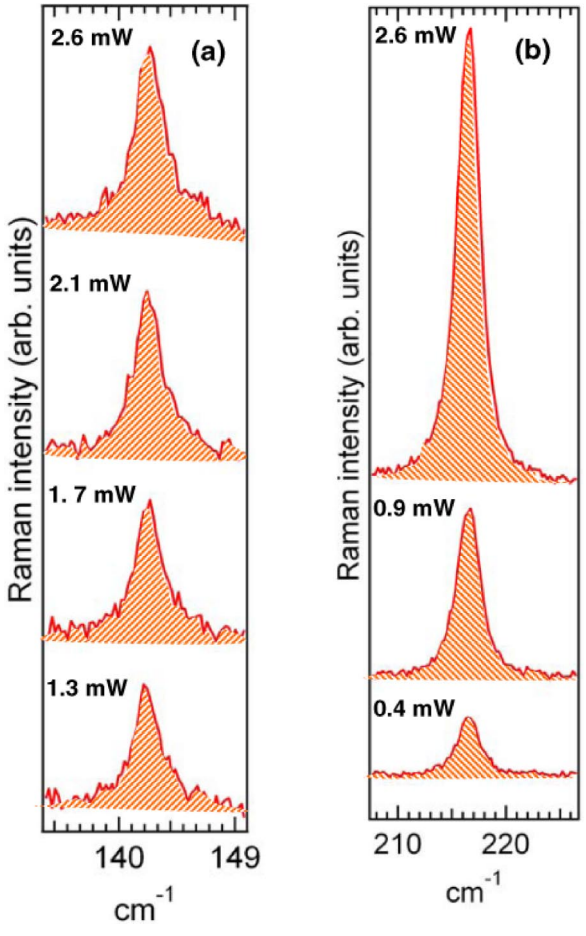

FIG. 1 (color online). Raman spectra around the RBM frequency for two suspended SWNTs collected for different incident laser powers. From the shape of the tangential band near 1590 cm^{-1}, panels (a) and (b) are assigned to metallic and semiconducting SWNTs, respectively.

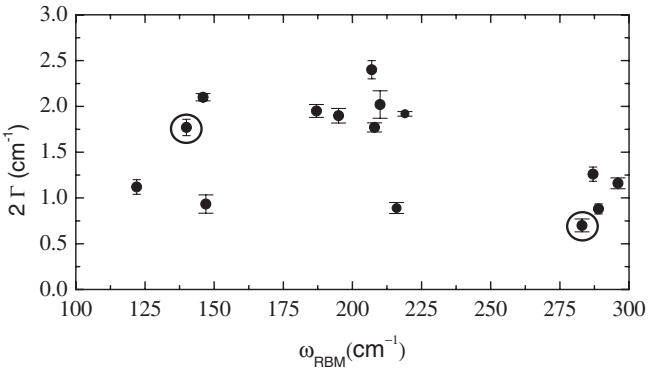

FIG. 2. Deconvoluted 2Γ (Lorentzian FWHM) values for several suspended SWNTs plotted versus the RBM frequency. The circled data points represent metallic SWNTs while the rest are semiconducting SWNTs.

$$k = \frac{\beta}{2b\kappa\pi^{3/2}} \int_0^{\sqrt{\ln 2}L/2r_0} \mathrm{erf}(\nu)d\nu,$$

where L is the length of the suspended portion of the nanotube and $b = 0.34$ nm is the tube wall thickness. The coefficient β is the fraction of light energy incident on the nanotube that is converted to thermal energy. We take $\beta = 0.38$, which results from assuming that the reflectivity of the nanotubes is the same as that of graphite, and that the absorbance is as measured by Islam *et al.* [12], but corrected by a factor (300/16) to account for the fact that the results of Ref. [12] correspond to an ensemble of nanotubes. The observed optical transition width for SWNT bundles is ~300 meV, whereas the corresponding width for an individual SWNT (as measured by resonance Raman scattering) is closer to 16 meV [13]. Recent near-field scanning optical microscopy results suggest $\beta = 0.58$, close to our selected value [14]. The above calculation assumes that all the absorbed light is converted to heat, which should be a good approximation for metals and less so for semiconducting tubes with short radiation lifetimes. However, given the large uncertainties in the computation of β we do not make any distinction between semiconducting and metallic SWNTs. Figure 3 shows the measured linewidths versus laser power as a function of nanotube length. The dotted lines correspond to Eq. (2) for nanotube lengths of $L = 2$–5 μm. As can be seen in the figure, most of the FWHM values agree well with predictions corresponding to SWNT lengths ranging between 2–5 μm over the trenches. The good agreement between the observed and calculated power dependences in Fig. 3 strongly suggests that the measured Raman linewidths represent the intrinsic anharmonic broadening for the RBM.

The fact that the instrinsic Raman linewidths are on the order of 1 cm^{-1} (5.3 ps) calls for an explanation of the observation of mode lifetimes of ~10 ns in the tunneling experiments. The standard perturbative approach for Raman linewidths assumes that the secondary phonons, i.e, the products of the Raman phonon decay, are in thermal equilibrium. This is justified in three-dimensional (3D) crystals because these phonons occupy a significant reciprocal space volume, [1] so that deviations from equilibrium for each individual mode are negligible. This condition is not met in suspended 1D SWNTs, where the phase space for decay products is reduced to a few discrete points.

We have run numerical simulations of phonon decay that take into account the presence of nonequilibrium secondary phonons. An excess population δn_0 of primary phonons of frequency ω_0 (in our case $\omega_0 = \omega_{\mathrm{RBM}}$) decays into pairs of phonons of frequency $\omega_1 = \omega_0/2$. (The assumption of equal frequency for the two secondary phonons is not critical but simplifies the math). This decay process creates an out-of-equilibrium population δn_1 of secondary phonons, which further decays into pairs of tertiary phonons of frequency $\omega_2 = \omega_1/2$. The tertiary phonons are assumed to be in thermal equilibrium. If we apply Fermi's Golden Rule to the third-order lattice anharmonic

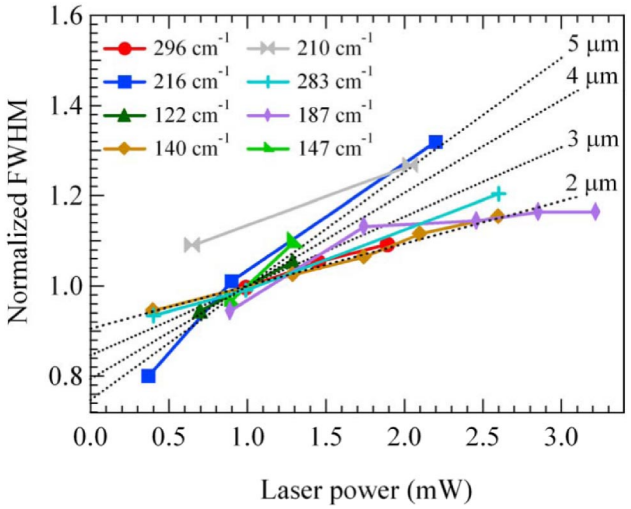

FIG. 3 (color online). Normalized linewidth versus incident total laser power P (The normalized linewidth is defined as the Lorentzian FWHM at P divided by the FWHM at $P = 1$ mW). The lines show predictions from Eq. (2) for different values of L.

Hamiltonian, we obtain the set of coupled equations

$$\begin{aligned}\frac{d(\delta n_0)}{dt} &= -\frac{1}{\tau_{01}}(1+2n_1)\delta n_0 + \frac{2}{\tau_{01}}(n_1 - n_0)\delta n_1 \\ \frac{d(\delta n_1)}{dt} &= \frac{1}{p\tau_{01}}(1+2n_1)\delta n_0 - \left[\frac{1}{\tau_{12}}(1+2n_2)\right. \\ &\quad \left. + \frac{1}{p\tau_{01}}(n_1 - n_0)\right]\delta n_1,\end{aligned} \tag{3}$$

where we have neglected terms that are nonlinear in δn_0, δn_1 [15]. Here τ_{01} is the decay rate for primary into secondary phonons and τ_{12} is the decay rate for secondary into tertiary phonons. The parameter p counts the number of pairs of secondary phonons that satisfy the energy and crystal momentum conservation rules. If we consider a $\boldsymbol{k} = \boldsymbol{0}$ phonon in a 3D crystal decaying into two equal-frequency acoustic phonons with linear dispersion, the possible wave vectors of the decay phonons form a spherical shell in $\boldsymbol{k}$-space. By contrast, for the same conditions in a 1D crystal the wave vectors of the decay products are reduced to a single $(\boldsymbol{k}, -\boldsymbol{k})$ pair. Thus in 3D solids we usually have $p \gg 1$, whereas for 1D systems we expect $p \sim 1$. If we set $\delta n_1 = 0$, Eq. (3) is equivalent to Eq. (1), with $2\Gamma = 1/\tau_{01}$. Figure 4(a) shows calculations of δn_0 for $\tau_{12} = 500\ \tau_{01}$, a reasonable choice if the secondary phonons are acoustic phonons with lifetimes much longer than the optical phonon lifetime [16]. For the solid line, the initial condition is $\delta n_0 = 0.1$, $\delta n_1 = 0$ and $p = 2$. We notice that there is a fast initial decay, determined by τ_{01}, followed by a much slower decay that is dominated by τ_{12}. This is caused by the long-lived secondary phonons recombining and generating new primary phonons. The reason why the lifetime of the secondary decay products comes to determine the lifetime of the primary phonons is the decay bottleneck induced by the low value chosen for the parameter p. If we increase this value, as done for the

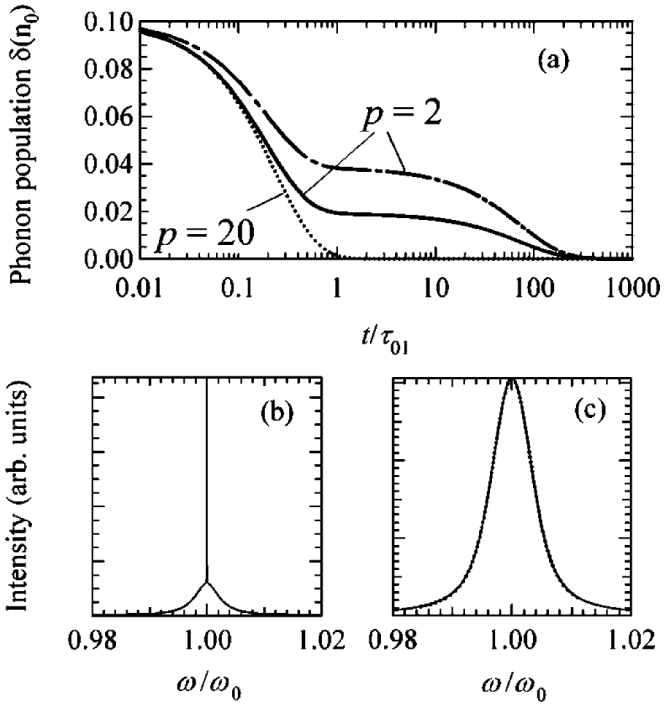

FIG. 4. (a) Solid line: Raman phonon population decay under conditions that create a decay bottleneck due to the reduced phase space for secondary phonons ($p \sim 2$). This is the most realistic assumption for carbon nanotubes, Dotted line: Raman phonon population decay under conditions in which the decay bottleneck is negligible ($p \gg 1$), Dashed-dotted line: Raman phonon population decay when the secondary phonons are also created by the external perturbation, as could be the case in a tunneling experiment; (b) predicted Raman spectrum corresponding to the solid line in panel (a). The sharp central spike corresponds to the long lifetime tail in panel (a); (c) Solid line: Modeled observed Raman spectrum obtained from convoluting the spectrum in panel (b) with a Gaussian function that represents a typical instrumental resolution. Dotted line: Fit of the solid line using a Voigt profile, as typically done to extract the Lorentzian linewidth from the observed experimental line shape. The extracted Lorentzian linewidth represents the broad tail in panel (b), whereas information from the central spike is lost in the convolution process. Thus it is not possible to detect the long lifetime component in a Raman experiment.

dotted line, the effect of the secondary phonons vanishes and the decay is completely determined by the shorter lifetime τ_{01} of the primary phonons.

The scenario just depicted offers a natural interpretation for the discrepancy between the Raman and tunneling measurements. In Fig. 4(b) we show the calculated Raman line shape (using the fluctuation-dissipation theorem) corresponding to the solid line decay pattern in Fig. 4(a). It has a very sharp central maximum, corresponding to the long lifetime τ_{12}, and much broader tails corresponding to the short lifetime τ_{01}. However, the *observed* Raman spectrum is a convolution of the intrinsic line shape with the instrument's resolution function, and this is depicted in Fig. 4(c). Here the central spike has essentially vanished, and if we fit the convoluted line shape with a standard Voigt profile, we obtain for the Lorentzian FWHM $2\Gamma = 0.98/\tau_{01}$. In other words, a Raman spectrum under these conditions would measure the short lifetime τ_{01}, whereas the tunneling experiments of Ref. [2], would see the much longer lifetime τ_{12}. The apparent discrepancy between the two types of measurements is further enhanced if we consider the fact that in a tunneling experiment—as opposed to a Raman process—there is no strong selection rule restricting the phonons that can be activated. Therefore, if the tunneling event generates primary *and* secondary phonons, the presence of these secondary phonons may contribute to a further reduction of the decay of the primary phonon. This effect is simulated by the dash-dotted line in Fig. 4(a), which was computed with initial conditions $\delta n_0 = 0.1$, $\delta n_1 = 0.5$.

In summary, we have presented evidence for the measurement of intrinsic Raman linewidths in suspended SWNTs, and we have identified a 1D phonon decay bottleneck as a plausible explanation for the apparent discrepancy between Raman and tunneling measurements. The selection rules imposed by the low dimensionality hinder the thermalization of phonons and should affect the transport properties of carbon nanotubes. The existence of hot phonons effects in carrier transport is evident from current-voltage measurements [10,17]. Similarly, the strong temperature dependence of the thermal conductivity at temperatures corresponding to optical phonons [18] suggests that hot phonons effects may also play a role in heat transport phenomena.

[1] A. Debernardi, S. Baroni, and E. Molinari, Phys. Rev. Lett. **75**, 1819 (1995).
[2] A. J. LeRoy, S. G. Lemay, J. Kong, and C. Dekker, Nature (London) **432**, 371 (2004).
[3] H. Son *et al.*, Appl. Phys. Lett. **85**, 4744 (2004).
[4] A. Hartschuh, H. N. Pedrosa, L. Novotny, and T. D. Krauss, Science **301**, 1354 (2003).
[5] A. Jorio *et al.*, Phys. Rev. B **66**, 115411 (2002).
[6] Y. S. Lim *et al.*, arXiv:cond-mat/0606396.
[7] S. Huang, X. Cai, and J. Liu, J. Am. Chem. Soc. **125**, 5636 (2003).
[8] R. Pfeiffer *et al.*, Phys. Rev. Lett. **90**, 225501 (2003).
[9] R. F. Wallis and M. Balkanski, *Many Body Aspects of Solid State Spectroscopy* (North-Holland, Amsterdam, 1986).
[10] E. Pop *et al.*, Phys. Rev. Lett. **95**, 155505 (2005).
[11] P. Kim *et al.*, Phys. Rev. Lett. **87**, 215502 (2001).
[12] M. F. Islam, D. E. Milkie, C. L. Kane, A. G. Yodh, and J. M. Kikkawa, Phys. Rev. Lett. **93**, 037404 (2004).
[13] A. Jorio *et al.*, Phys. Rev. B **63**, 245416 (2001).
[14] W. Zhang *et al.*, Scanning Suppl. I, **26**, I21 (2004).
[15] S. Jursenas, A. Zukauskas, and R. Baltramiejunas, J. Phys. Condens. Matter **4**, 9987 (1992).
[16] A. Berke, A. P. Mayer, and R. K. Wehner, J. Phys. C **21**, 2305 (1988).
[17] M. Lazzeri and F. Mauri, Phys. Rev. B **73**, 165419 (2006).
[18] S. Berber, Y.-K. Kwon, and D. Tomanek, Phys. Rev. Lett. **84**, 4613 (2000).